PAPER

Onset of tearing modes in plasma termination on JET: the role of temperature hollowing and edge cooling

IOP Publishing | Bureau International des poids et Mesures Nuclear Fusion

Nucl. Fusion **61** (2021) 046020 (12pp) https://doi.org/10.1088/1741-4326/abe3c7

Onset of tearing modes in plasma termination on JET: the role of temperature hollowing and edge cooling

G. Pucella[1,*], P. Buratti[1], E. Giovannozzi[1], E. Alessi[2], F. Auriemma[3], D. Brunetti[4], D.R. Ferreira[5], M. Baruzzo[1], D. Frigione[6], L. Garzotti[4], E. Joffrin[7], E. Lerche[8], P.J. Lomas[4], S. Nowak[2], L. Piron[9], F. Rimini[4], C. Sozzi[2], D. Van Eester[8] and JET Contributors[a]

[1] ENEA, Fusion and Nuclear Safety Department, C.R. Frascati, Italy
[2] ISTP, Consiglio Nazionale delle Ricerche, Milano, Italy
[3] ISTP, Consiglio Nazionale delle Ricerche, Padova, Italy
[4] Culham Centre for Fusion Energy, Abingdon, United Kingdom of Great Britain and Northern Ireland
[5] IPFN/IST, University of Lisbon, Lisbon, Portugal
[6] Università degli Studi di Roma 'Tor Vergata', Roma, Italy
[7] CEA, IRFM, Saint-Paul-lez-Durance, France
[8] Laboratory for Plasma Physics-Ecole Royale Militaire, Brussels, Belgium
[9] Università degli Studi di Padova, Padova, Italy

E-mail: gianluca.pucella@enea.it

Received 1 October 2020, revised 11 January 2021
Accepted for publication 5 February 2021
Published 12 March 2021

Abstract

In this work the onset of tearing modes in the termination phase of plasma pulses on JET is investigated. It is shown that the broadening or the shrinking of the current density profile, as a consequence of a core hollowing or an edge cooling of the electron temperature profile, strongly increases the probability of destabilizing a 2/1 tearing mode also in absence of an external trigger (e.g. a sawtooth crash). Two parameters are defined to highlight changes in the shape of the temperature profile that can lead to MHD instabilities and an empirical stability diagram is introduced into the space of the two new parameters. A large data-set of pulses carried out in the high-current scenario at JET with ITER-like wall is analyzed and criteria for the development of disruption alerts based on the two risk indicators for MHD instabilities are discussed, taking into account the different dynamics of the observed phenomena leading to the onset of 2/1 tearing modes.

Keywords: tearing modes, plasma termination, JET, temperature hollowing, edge cooling, onset

(Some figures may appear in colour only in the online journal)

1. Introduction

The capability to terminate plasma pulses safely is an important goal towards the optimization of an operating scenario in a tokamak. The occurrence of a disruption, namely a fast loss of plasma confinement followed by a quench of the plasma current, poses serious problems in tokamak devices. For the scenario development they limit the range of accessible plasma parameters, while from the operational point of view the release of a large amount of energy in a short time interval could result in large thermal and electromagnetic loads on the vacuum vessel and plasma facing components. For these reasons, it is of great importance to study the physical

* Author to whom any correspondence should be addressed.
[a] See Joffrin *et al* 2019 (https://doi.org/10.1088/1741-4326/ab2276) for the JET Contributors.

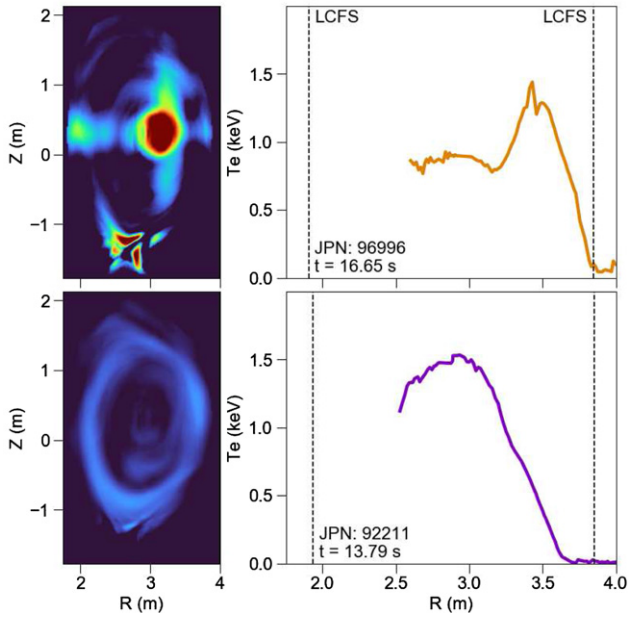

Figure 1. Tomographic reconstructions of the plasma radiation profile (left) and electron temperature profiles from ECE radiometry (right) for the termination phase of two pulses characterized by an increased radiation emission in core (JPN 96996, top) and edge (JPN 92211, bottom) plasma, respectively. The same dynamic range of 1 MW m^{-3} has been adopted for the two tomographic reconstructions on the left figures. Vertical dashed lines on the right figures correspond to the positions of the last closed flux surface.

phenomena involved in the disruptions and to develop disruption precursors for avoidance or mitigation actions [1–5]. Among the possible causes of disruptions, the development of tearing modes [6] inside the plasma is undoubtedly one of the most worthy of attention, due to the deleterious effects of growing magnetic islands on the flux surface structure. In particular, the termination phase, characterized by the reduction of auxiliary heating, often presents $m/n = 2/1$ tearing modes (m and n are the poloidal and toroidal mode numbers, respectively) [7], leading in most cases to disruption [8, 9]. It is worth noting that an increased radiation emission in core or edge plasma, leading to temperature hollowing and edge cooling, respectively, is usually observed before the onset of tearing modes in plasma termination. Tomographic reconstructions of the plasma radiation profile and electron temperature profiles from ECE radiometry are reported in figure 1 for two pulses characterized by an increased radiation emission in core (JPN 96996, top) and edge (JPN 92211, bottom) plasma, respectively. Qualitatively, both temperature hollowing and edge cooling can destabilize a $2/1$ tearing mode as a consequence of an increase of the current density gradient near the mode resonant surface. In the first case, the hollowing of the temperature profile could lead to a broadening of the current density profile, which would result flat or marginally hollow near the magnetic axis, but with higher gradient near the mode resonant surface, so the cause of the instability would be the broadening of the current density profile from inside [7, 10]. In the second case, the contraction of the temperature profile leads to a shrinking of the current density profile, so the cause of the instability would be essentially the erosion of the current density profile from outside [11].

In the present work the effect of changes in the shape of the electron temperature profile on mode onset is analyzed for the termination phase of high-current plasma pulses performed at JET with ITER-like wall. In section 2 the possible explanation for the mode onset in terms of a linear destabilization of tearing modes as a consequence of broadening or shrinking of the current density profile in presence of temperature hollowing or edge cooling, respectively, is confirmed through interpretative simulations and stability analysis of real pulses representative of the two scenarios, whilst the subsequent mode growth is delegated to non-linear mechanisms. In section 3 two parameters are defined on the basis of ECE radiometry measurements to characterize the shape of the electron temperature profile and the time evolution of such parameters is studied for some representative pulses to highlight their correlation with mode onset and dynamics in disruptive pulses. In section 4 a large data-set including both non-disruptive and disruptive pulses is analyzed to estimate the characteristic time interval between temperature hollowing and edge cooling processes and the locking of the increasing magnetic island [12], and the possibility to obtain disruption precursors (nay mode onset precursors) based on the two parameters indicating changes in the shape of the electron temperature profile is explored. Finally, in section 5 the conclusions are discussed and the perspectives for future works are illustrated.

2. Tearing mode activity

Tearing modes characterized by different poloidal and toroidal mode numbers are sometimes observed during the stationary phase of plasma pulses at JET, often triggered by external events such as sawtooth crashes, fishbone activities and perturbations associated with edge localized modes. Tearing modes are also observed in the termination phase of disruptive pulses. However, due to the reduction of the additional power, the above trigger mechanisms are rarely present, whilst an increased radiation emission from core or edge plasma, leading to temperature hollowing and edge cooling, respectively, is observed before the onset of the modes.

It is well known that the destabilization of a classical tearing mode in a tokamak is driven by the radial gradient of the toroidal current density profile, which is related to the free energy available for the modes [13]. An important role is played by the current density gradient near the mode resonant surface, where $q = m/n$, even though the mode stability generally involves the global shape of the current profile [14–16]. It is worth noting that in the termination phase the current profile is dominated by the ohmic contribution and the resistivity is high due to the low temperature ($\eta \approx Z_{\mathrm{eff}}/T_{\mathrm{e}}^{3/2}$, where Z_{eff} and T_{e} are the effective charge and the electron temperature, respectively), so the current profile changes on a relatively short resistive diffusion time scale ($\tau_{\mathrm{R}} \approx \mu_0 L^2/\eta$, where L is the characteristic spatial scale involved) reflecting the changes in the electron temperature profile. The destabilization of 2/1 tearing modes by changes in the current density

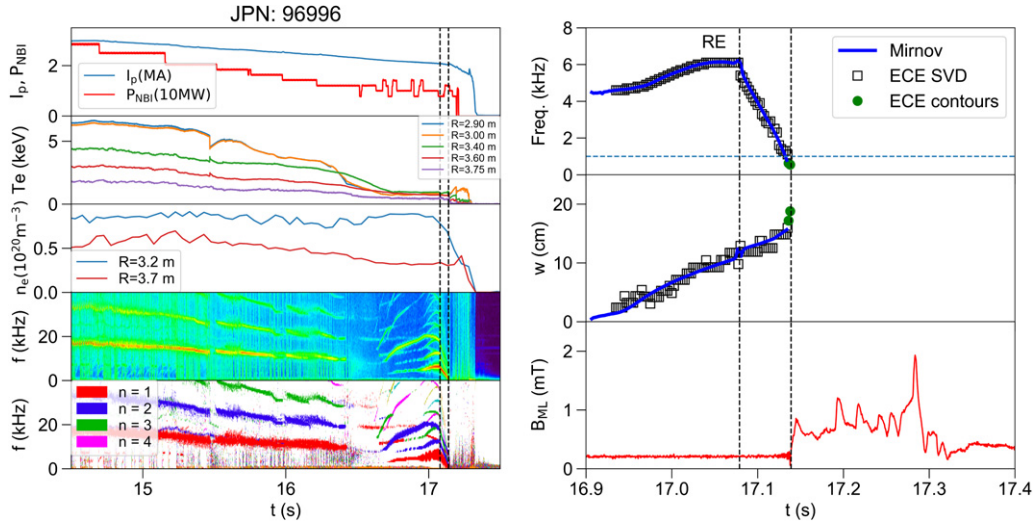

Figure 2. (Left) Time traces of the plasma termination of a pulse with temperature hollowing only. From top to bottom: plasma current and neutral beam power, electron temperature at different radii, electron density at different radii, spectrogram of a magnetic pick-up coil, toroidal mode number analysis from a magnetic pick-up coil array. (Right) Time traces of the $n = 1$ mode frequency and island width from Mirnov coils and from SVD analysis of ECE channels acquired at 200 kHz, and of the $n = 1$ mode lock amplitude from saddle flux loops for the last 400 ms to disruption. A direct estimation of the island width from ECE contours for the last 5 ms to mode lock has been also added (green symbols). JPN 96996.

profile in plasma termination on JET is analyzed in the next paragraphs.

2.1. Experimental observations

Both destabilization paths mentioned before, namely the shrinking of the current density profile as a consequence of edge cooling and the broadening of current density profile due to temperature hollowing, can occur during the JET plasma termination. Their percentage incidence strongly depend on the operational scenario. Lower density and a flatter safety factor profile are prone to develop tearing modes as a consequence of a temperature hollowing associated with core impurity accumulation, whilst for peaked safety factor profiles and higher density the tearing modes are mainly caused by edge cooling as a consequence of the higher peripheral density in the termination phase. The formation of an outer radiative blob due to impurities accumulated in the low field side can also be responsible for an edge cooling.

In figure 2 (left) time traces of a representative pulse (JPN 96996) characterized by temperature hollowing only, without edge cooling before the mode onset, are shown. The temperature hollowing is associated with an increased radiation emission in core plasma, as highlighted by the tomographic reconstructions of the plasma radiation profile reported in figure 1 (top). In this pulse the heating power starts to be turned off from 14.7 s and the plasma current is ramped-down. A hollowing of the electron temperature profile begins around 16.3 s, approximately 1 s before the disruption, as highlighted by the crossing of temperature lines corresponding to different radii. This behavior is likely due to heavy impurity accumulation, which is a crucial point in JET with ITER-like wall [17]. In fact, an impurity accumulation was also observed in JET − C, but the influx of carbon did not affect the electron temperature profile as much as core radiating high-Z materials such as tungsten or nickel, which make the aspect of core impurity accumulation more serious in JET − ILW. Following the change in the temperature profile, an increase in central safety factor is expected, as confirmed by disappearing at 16.42 s of the long lasting continuous $1/1$ mode, related to $q = 1$ magnetic surface in the plasma (red line in the bottom panel). Afterwards a sequence of mode onsets with decreasing toroidal mode number n is observed in the bottom panel: $5/4$ at 16.62 s, $4/3$ at 16.63 s, $3/2$ at 16.68 s. All these modes are characterized by increasing frequencies, suggesting rational surfaces moving inward as a consequence of a q-profile modification following the temperature hollowing. A $2/1$ mode is observed in the outer part of the plasma starting from 16.75 s with slightly increasing frequency; after a reconnection event (RE) at 17.08 s the mode locks at 17.14 s (this sequence is typical for this kind of pulses) and finally the plasma disrupts. The temporal evolution of the $n = 1$ mode frequency and island width w, and of the mode lock amplitude from saddle flux loops (mounted on the outside of the vacuum vessel at the low-field-side) is reported in figure 2 (right) for the last 400 ms to disruption. The island growth, as roughly estimated by the poloidal magnetic perturbations measured by Mirnov coils ($w \propto \sqrt{B_{\theta 1}}$ [18]), is algebraic in the first phase, as confirmed by singular value decomposition [19] analysis of electron temperature fluctuations (ECE channels acquired at 200 kHz), whilst a faster growth seems to characterize the last phase before locking. It is worth noting that all $2/1$ modes destabilized as a consequence of temperature hollowing are characterized by a fast initial mode rotation.

In figure 3 (left) time traces of a representative pulse (JPN 92211) characterized by edge cooling only are shown. The edge cooling is associated with an increased radiation emission in edge plasma, as highlighted by the tomographic

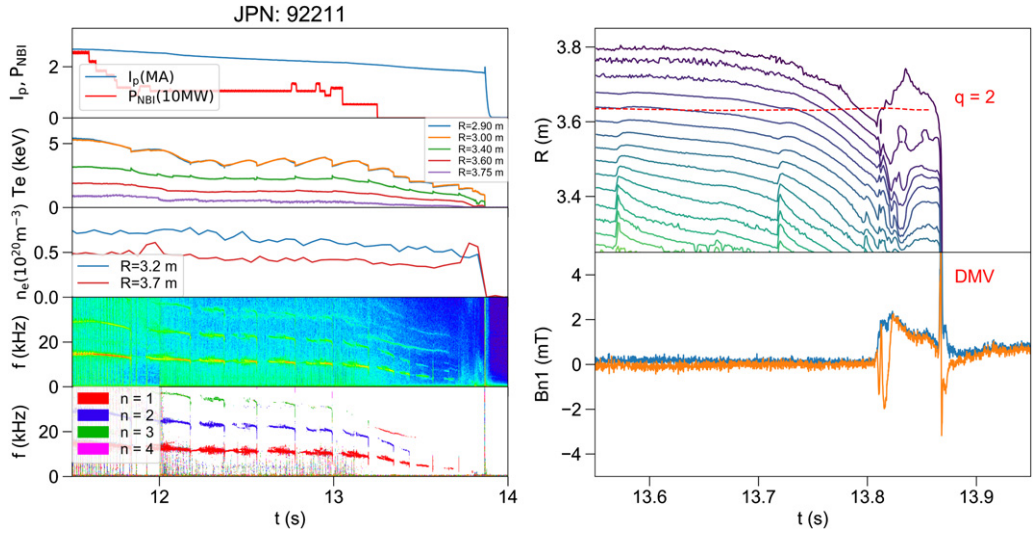

Figure 3. (Left) Time traces of the plasma termination of a pulse with edge cooling only. From top to bottom: plasma current and neutral beam power, electron temperature at different radii, electron density at different radii, spectrogram of a magnetic pick-up coil, toroidal mode number analysis from a magnetic pick-up coil array. (Right) Time traces of the electron temperature contours (top) and of $n = 1$ mode amplitude and sine component on internal discrete coils (bottom) for the last 300 ms to disruption. JPN 92211.

reconstructions of the plasma radiation profile reported in figure 1 (bottom). In this pulse the heating power starts to be turned off from 11.6 s and the plasma current is ramped-down, but the electron temperature profile remains peaked, as highlighted by sawtooth crashes in the inner electron temperature channels. In this phase only the precursor of the sawtooth activity is observed in the spectrogram. An edge cooling process starts from 13.68 s, as visible by outer electron temperature channels, and a hint of $n = 1$ MHD activity can be seen in the spectrogram from 13.82 s at very low frequencies, where Mirnov coils do not provide good signals due to low frequency drift. Additional signals are reported in figure 3 (right) for the last 300 ms to disruption. On the top panel, the time traces of the electron temperature contours from electron cyclotron emission radiometry confirm the start of edge cooling from 13.7 s and show some rapidly increasing variations (with a sort of divergent behavior) from 13.8 s, when the edge cooling affects the region around the $q = 2$ surface ($R \approx 3.63$ m). On the bottom panel the $n = 1$ mode amplitude (blue line) and sine component (orange line) on internal discrete coils (an array of coils slower than the Mirnov coils but with better drift compensation) show some oscillations associated to the magnetic island rotation and then a saturation, while the thermal quench is induced by disruption mitigation valve (DMV) intervention, as indicated by the corresponding spikes in the mode amplitude signal. Usually $2/1$ modes destabilized as a consequence of edge cooling make only a few turns before locking, whilst only few cases with a short phase of fast initial mode rotation and very few cases with locked birth are observed. It is worth noting that in case of peaked electron temperature profiles, the 2/1 modes generally tend to saturate.

The two pulses shown are representative of the general chain of events leading to the onset of $2/1$ tearing modes in termination phase when temperature hollowing or edge cooling occur, but clearly they not catch all the possible behaviors. In case of $2/1$ modes induced by temperature hollowing, after the disappearing of the $q = 1$ magnetic surface, some pulses present spontaneous tearing modes as shown in figure 2; other pulses are similarly characterized by a sequence of modes with decreasing toroidal mode number n, but each mode is triggered by a RE. In case of $2/1$ modes induced by edge cooling, the mode onset can occur with differently shaped electron temperature profiles. The example presented in figure 3 is representative of cases where the mode onset occur with peaked electron temperature profiles. However, there are several cases in which the mode onset occur with hollow profiles. In these cases the pulse has all the signatures of temperature hollowing, but final collapse appears to be from edge. Coming back to the two scenarios where temperature hollowing or edge cooling occur separately, two open questions need to be answered: (1) following changes in the electron temperature profile, is the current density profile changing before the $2/1$ mode onset? (2) are the current density profile changes heading in the direction of a more unstable MHD scenario? The next two sections are therefore devoted to providing a quantitative answer to these two crucial questions.

2.2. TRANSP simulations

Interpretative TRANSP [20] simulations are carried out for the two pulses mentioned before, representative of the temperature hollowing (JPN 96996) and edge cooling (JPN 92211) scenario, respectively, in order to answer the questions in the previous section. The simulations have been performed providing TRANSP with electron temperature and density profiles as measured by high resolution Thomson scattering (HRTS), and $T_i = T_e$ is assumed. The effective charge temporal evolution is prescribed with the visible Bremsstrahlung data assuming a uniform Z_{eff} profile. The profiles are mapped on the flux coordinate ρ_{tor}, i.e. square root of normalized toroidal flux, which is calculated by EFIT [21]. EFIT provides also the initial

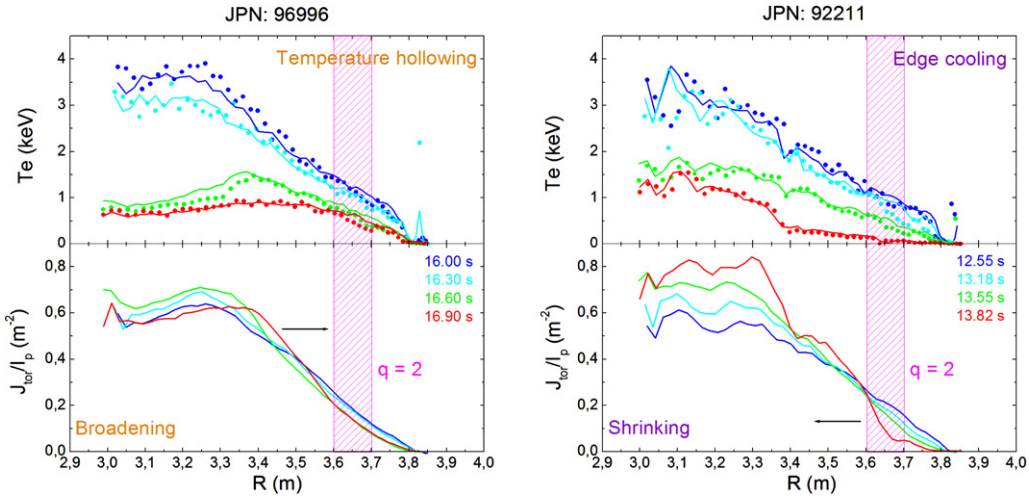

Figure 4. Time evolution of electron temperature (top) and current density (bottom) profiles, from TRANSP simulations, for the termination phase of JPN 96996 with temperature hollowing only (left) and JPN 92211 with edge cooling only (right). Experimental data from HRTS are reported as solid points in top panels.

condition for the plasma equilibrium (i.e. safety factor profile, surfaces geometry, etc.) which is then evolved by the TRANSP internal inverse solver TEQ [22]. The current density profiles are calculated at each time step solving to the poloidal field diffusion equation, including the ohmic, bootstrap and current driven contribution, according with the driving terms and the classical Spitzer resistivity [18]. It is important to note that, in the analyzed time window that corresponds to the terminal phase of the plasma, the plasma current is dominated by the ohmic term. The Spitzer resistivity has been preferred, based on the observation that the use of neoclassical resistivity in the modeling systematically overestimates the rates of current profile evolution during current ramp-up or ramp-down [23]. Tests with different choices of the resistivity give results in qualitative agreement with what obtained using the Spitzer formula. The simulations, besides calculating the internal current density profiles, provide values of local and global quantities to be compared with the experimental data, to assess the reliability of the computation: in particular the stored energy, total neutrons and line integral density are within 10% of the corresponding experimental values, confirming the quality of the present approach [24].

The time evolution of electron temperature and current density profiles is reported for the two pulses in figure 4. Changes in current density profile generally reflect the expected evolution following changes in the electron temperature profile, with time delays associated with the effective resistive diffusion times. In particular, for JPN 96996, characterized by a temperature hollowing beginning around 16.3 s, the current density profile seems to start changing between 16.6 s and 16.8 s, so an effective resistive diffusion time of the order of 0.3–0.5 s can be estimated at first glance. It is worth noting that only a broadening of the current density profile is observed in this case, without a substantial hollowing of the central region. This could also be due to the flat effective charge profile Z_{eff} considered in the simulation. More detailed analysis will be performed in near future with the introduction of shaped effective charge profile, reflecting the impurity accumulation in pulses with temperature hollowing. However, we will see in the next paragraph that the shaping of the current density profile here evaluated is sufficient to explain a linear destabilization of the 2/1 mode. For JPN 92211, characterized by an edge cooling beginning around 13.68 s, the current density profile seems to start changing between 13.71 s and 13.79 s, so an effective resistive diffusion time of the order of 30–110 ms can be estimated at first glance. The spread in this estimation is due to the fact that the pulse is characterized by sawtooth activity, so the comparison between current density profiles has been made considering only times corresponding to a distinct phase of the sawtooth activity, which has a period of order of 100 ms. An effective resistive diffusion time of the order of 50–100 ms can be estimated by removing the condition for selecting current density profiles. The accuracy of the estimation is now associated to the temporal resolution of the HRTS diagnostics, which is acquired at 20 Hz. Faster temperature measurements, like ones provided by ECE radiometry, would give a more precise estimate of the effective resistive time.

It is worth noting that in both cases a general decrease in the electron temperature values is observed at different radii (top panels in figure 4), due to the global plasma cooling during the termination phase. This is the reason why the current density profiles (bottom panels in figure 4) have been normalized to the total plasma current at their respective times, highlighting the different region affected by changes in the local resistivity. Concerning the stability of the 2/1 tearing modes as a consequence of changes in the current density profile, in both pulses an increase in the gradient in the $q = 2$ region is observed, qualitatively supporting the hypothesis of an ongoing destabilization process.

2.3. *Tearing stability analysis*

Linear stability analyses have been performed for the two pulses JPN 96996 and JPN 92211 for the time intervals of figure 4 (i.e. before the observation of large magnetic islands),

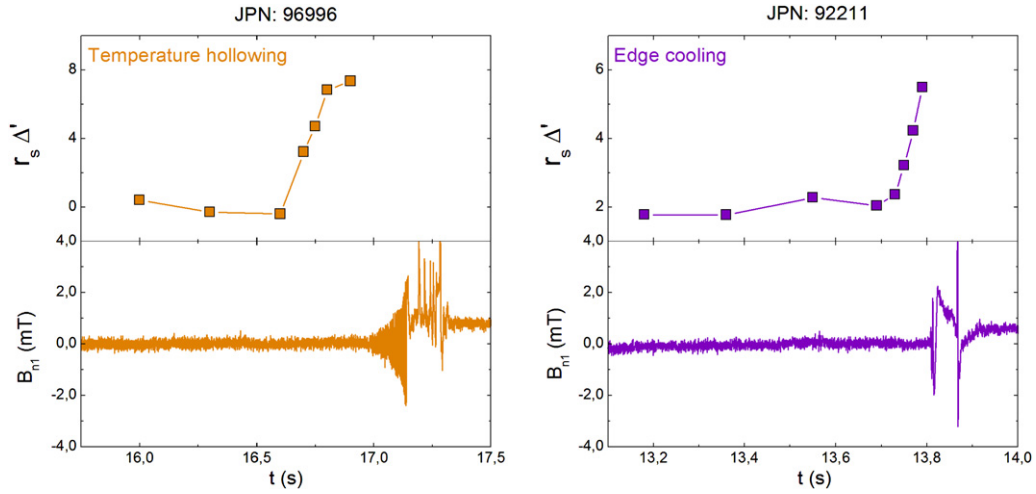

Figure 5. Time traces of the tearing stability index Δ' (top) and of sine component of $n = 1$ magnetic signals on internal discrete coils (bottom) for the termination phase of JPN 96996 with temperature hollowing only (left) and JPN 92211 with edge cooling only (right).

by solving the equation for the perturbed radial magnetic field B_{r1} [25] in the zero pressure limit:

$$\frac{\mathrm{d}}{\mathrm{d}r}\left[\left\langle\frac{g_{\theta\theta}}{\sqrt{g}}\right\rangle\frac{\mathrm{d}}{\mathrm{d}r}\left(rB_{r1}\right)\right] = \left[\left\langle\frac{g_{rr}}{\sqrt{g}}\right\rangle m^2 + \frac{q\mu_0}{\left(1-nq/m\right)}\frac{\mathrm{d}}{\mathrm{d}r}\left\langle\frac{j_{\mathrm{tor}}}{B_{\mathrm{tor}}}\right\rangle\right]\left(rB_{r1}\right) \quad (1)$$

with perfectly conducting wall boundary condition. In the equation above r is the radial coordinate defined from the normalized poloidal flux, q is the safety factor, j_{tor} and B_{tor} are the toroidal current density and magnetic field respectively, g_{rr} and $g_{\theta\theta}$ are the metric tensor coefficients, with $\sqrt{g}$ the Jacobian and the poloidal average denoted by angular brackets. Note that the equation above reduces to the cylindrical version when $g_{rr} = 1$, $g_{\theta\theta} = r^2$ and $\sqrt{g} = rR_0$. The profiles for the physical quantities appearing in equation (1) are obtained from toroidal equilibria computations performed with CHEASE code [26] based on TRANSP outputs. In the zero pressure approximation, the linear stability of the tearing mode is determined by the parameter Δ' [27] defined as the jump of the logarithmic derivative of perturbed radial magnetic field B_{r1} across the mode resonant surface, viz $\Delta' \equiv \left(\mathrm{d}\ \ln B_{r1}/\mathrm{d}r\right)_{s_+} - \left(\mathrm{d}\ \ln B_{r1}/\mathrm{d}r\right)_{s_-}$ where the subscripts s_+ and s_- denote the two sides of the mode resonant surface. For vanishing pressure gradients, Δ' is proportional to the change in magnetic energy associated with the magnetic perturbation [13, 16] so that higher values of Δ' correspond to more unstable scenarios. We point out that Δ' must exceed a positive threshold in order to destabilize the mode when the stabilizing contributions due to pressure and curvature effects are taken into account [28–30].

The results of the calculation of Δ', based on the reconstructed equilibria of pulses JPN 96996 and JPN 92211, are reported in figure 5 where the Δ' time traces are compared with the sine components of $n = 1$ magnetic signals on internal discrete coils. In both cases Δ' remains almost constant when no coherent oscillations are observed, indicating that magnetic islands are not present or their amplitude is so small as to be undetectable ($w < 0.5$ cm, which is the value associated with the noise of pick-up coils). In this phase also relatively small stabilizing contributions due to pressure and curvature effects are sufficient to justify the tearing stability. An increase in Δ', due to current re-distributions, is observed shortly before the mode onset. We note that it is likely that the stabilizing contributions due to pressure and curvature effects do not increase during the termination phase as they are directly proportional to pressure and conductivity (both decreasing). This suggests the presence of a distinct positive threshold in Δ', reinforcing the hypothesis of an ongoing destabilization process, which is a relevant point given the absence of evident external triggers in the terminal phase of the two analyzed pulses (a simple model based upon an analytical expression for the current density profile is reported in the appendix A). More detailed linear stability analysis will be performed in near future evaluating also the pressure and curvature effects, here taken into account only qualitatively for the interpretation of the destabilization process.

It is well known that the very early stage of the island evolution in collisional and semi-collisional regimes, which are appropriate to these low-temperature phases of the pulses, is characterized by an exponential growth [31, 32]. However, when the island width exceeds the resistive layer width (of the order of few millimeters [31, 32]), non-linear currents dominate over the inertia and the growth slows from exponential to algebraic (figure 2, right). The non-linear mode growth is usually described by a modified Rutherford equation (MRE), where different contributions are take into account together with the non-linear formulation for Δ', i.e. $\Delta'(w)$, where the jump of the logarithmic derivative of B_{r1} is evaluated between the edges of the magnetic island [33–37]. In this framework, to start with a high value for $\Delta'(w)$ is an important boost for the first phase of the island evolution, which will be dominated by $\Delta'(w)$ term. We point out that a further non-linear destabilization process, due to radiation emission effects from impurities within the island [38, 39], has been proposed and invoked to

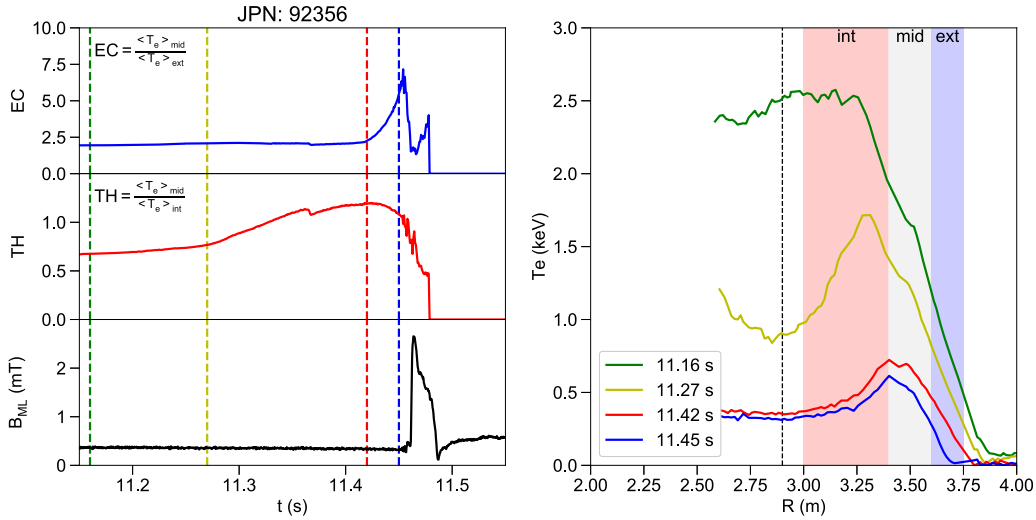

Figure 6. (Left) Temporal evolution of the two parameters TH and EC and of $n = 1$ mode lock amplitude in the termination phase of a JET pulse characterized by both temperature hollowing and edge cooling (JPN 92356). Temperature hollowing from 11.20 s; edge cooling from 11.42 s; mode lock at 11.45 s; disruption at 11.46 s. Dashed vertical lines correspond to times considered in the right figure. (Right) Temporal evolution of electron temperature profile from ECE radiometry for the last 300 ms to disruption. The regions considered for the definition of the two parameters TH and EC are indicated as shaded areas.

explain experimental results on the density limit [40–44]. In that model, when the net power flow into/out of the island becomes negative, namely the radiated power from the island exceeds the local ohmic heating power, the additional term in the MRE changes from being stabilizing to destabilizing and the island evolution obeys an asymptotic exponential law when the radiation drive term becomes the dominant one. This could contribute to explain the faster growth characterizing the last phase of the island evolution. Having said so, we stress that the non-linear radiation drive mechanism (and generally any MRE framework) requires the pre-existence of a finite size magnetic island, i.e. the island being linearly unstable or due to perturbation from external sources. In this sense, the radiation drive effect, acting through a helical current perturbation due to radiation from impurities within the island, has not to be confused with linear destabilization process, previously described, due to global changes in the current density profile as consequence of an increased radiation emission. Therefore, this suggests that the onset of the magnetic island during the termination phase without external triggers is entirely caused by a modification of the classical Δ' due to temperature, and consequently current density, variations, whilst the subsequent mode growth is delegated to non-linear mechanisms.

3. Temperature hollowing and edge cooling parameters

Following the picture of tearing modes generated by changes in the current density profile reflecting the changes in the electron temperature profile, two experimental parameters have been defined upon the electron temperature profile obtained by ECE radiometry to highlight the occurrence of the two possible phenomena leading to mode onset, namely the temperature hollowing and the edge cooling. In order to guarantee stable values apart from a change in the shape of electron temperature profile, the two parameters have been defined as ratio between two volume average temperatures, TH $\equiv \langle T_e \rangle_{V\mathrm{mid}} / \langle T_e \rangle_{V\mathrm{int}}$ and EC $\equiv \langle T_e \rangle_{V\mathrm{mid}} / \langle T_e \rangle_{V\mathrm{ext}}$, where the three volumes are defined considering the following major radii: $R = 3.00$–3.40 m for V_{int}, $R = 3.40$–3.60 m for V_{mid}, $R = 3.60$–3.75 m for V_{ext}. The radii of the internal volume have been chosen taking into account that the volume is used to highlight the temperature hollowing, likely due to core impurity accumulation, which usually affects the plasma region within the $q = 1$ surface. The radii of the external volume have been chosen so that the volume is entirely inside the pedestal region and taking into account the usual location of the $q = 2$ surface, which determines the limit for the erosion of the temperature profile before the mode onset in case of edge cooling. Based on the previous definitions, the TH parameter will increase in presence of a temperature hollowing, due to the greater decrease of $\langle T_e \rangle_{V\mathrm{int}}$ compared to $\langle T_e \rangle_{V\mathrm{mid}}$, while the EC parameter will increase in presence of edge cooling, due to the greater decrease of $\langle T_e \rangle_{V\mathrm{ext}}$ compared to $\langle T_e \rangle_{V\mathrm{mid}}$. The time delay between the changes of the two parameters and the onset of tearing modes will be related to the effective resistive diffusion time and to the time required to produce an unstable MHD scenario. The evolution of the two parameters and of $n = 1$ mode lock amplitude in the termination phase of a JET pulse (JPN 92356) characterized by both temperature hollowing and edge cooling is shown in figure 6 (left), highlighting a temperature hollowing and an edge cooling starting at about 300 ms and 60 ms to disruption, respectively. These results well reflect the temporal evolution of electron temperature profile reported in figure 6 (right).

In order to highlight the correlation between the changes in the shape of the electron temperature profile and the onset of tearing mode in plasma termination, the time evolution of the two parameters TH and EC has been evaluated for a dataset of 268 non-disruptive (136) and disruptive (132) pulses carried out at different plasma current values (from 2.5 to

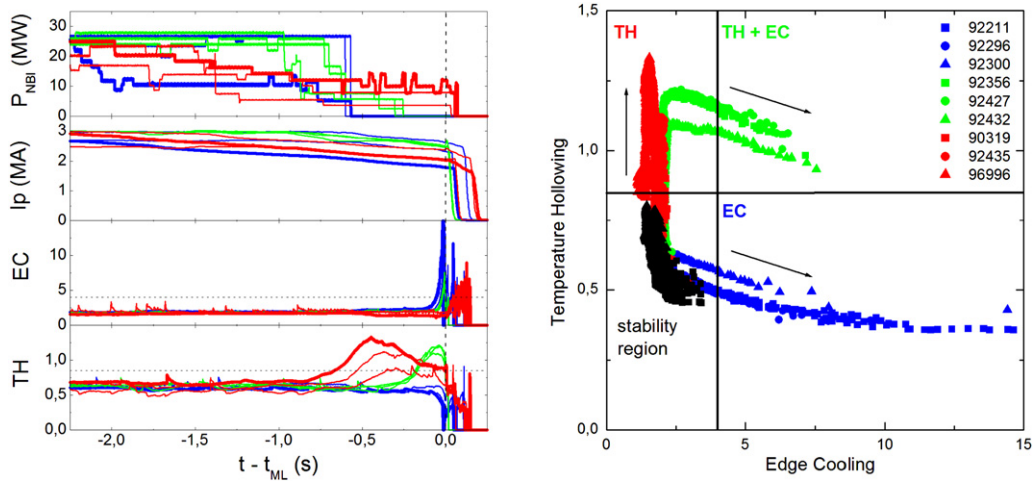

Figure 7. (Left) Time traces of 9 representative disruptive pulses performed in the baseline scenario at JET. From top to bottom: neutral beam power, plasma current, EC and TH parameters. Pulses are characterized by edge cooling only (blue lines), edge cooling and temperature hollowing (green lines) and temperature hollowing only (red lines). (Right) Paths of the 9 representative pulses on the EC–TH plane for the last 5 s to mode lock. Black symbols refer to EC–TH pairs for the time interval between 5 s and 1 s to mode lock.

3.7 MA) in the baseline scenario at JET [45] in the period 2016–2020. From the dataset analysis it is possible to see that non-disruptive pulses are generally devoid of temperature hollowing and edge cooling, with stable values for both parameters TH and EC. Only a 10% of pulses exhibits transient increases of one of the two parameters not followed by a disruption, sometimes related to spikes in pulses with full-size pellet injection, to edge localized modes or to non-disruptive MHD activity. As expected, disruptive pulses are characterized by constant values for both parameters TH and EC during the non-disruptive phase. Only in the last two seconds before the disruption an increase on one or both parameters is observed, although a 10% of pulses exhibits some increases too in advance of the disruption and not necessarily correlated with the effective chain of events leading to disruption. The same explanation given above is often valid for these cases.

To show some examples, time traces of nine representative disruptive pulses are reported in figure 7 (left), where a color code is used to highlight the simultaneous or separated occurrence of edge cooling and temperature hollowing: blue for pulses with only edge cooling, green for pulses with both edge cooling and temperature hollowing, red for pulses with only temperature hollowing before mode lock (JPN 92211 and JPN 96996, analyzed in section 2, are reported in the figure with blue and red thick lines, respectively). Time traces of TH and EC confirm the observation of constant values for both parameters (not strongly depending on heating power and plasma current) during the non-disruptive phase, with an increase of one or both parameters in the last second to mode lock, which is used as a reference (with a threshold for the magnetic measurement fixed at 0.5 mT) as it is directly related to the mode onset and growth up to a given amplitude. In particular, pulses with temperature hollowing or edge cooling develop 2/1 tearing modes in different characteristic times, of the order of 1 s and 100 ms, respectively. This behavior is highlighted in figure 7 (right), where the paths of the nine representative pulses on an 'EC-TH plane' are reported for the last

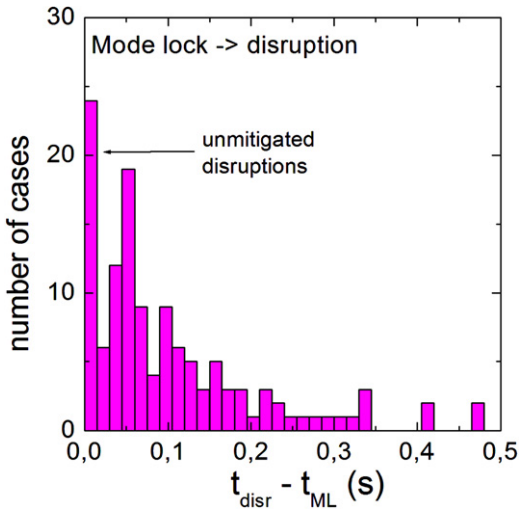

Figure 8. Distribution of the time interval between mode lock (t_{ML}) and disruption (t_{disr}) for the 132 disruptive pulses of the baseline dataset. The first bin (0–15 ms) correspond to unmitigated pulses (thermal quenches before DMV intervention). Longer delays correspond to low amplitude lock modes (triggering late the mitigation actions) and to pulses with sequences of soft disruptions.

5 s to mode lock. For the time interval between 5 s and 1 s to mode lock the EC–TH pairs for the nine pulses (indicated by black symbols) are located in a well defined quadrant where also the EC–TH pairs for non-disruptive pulses are usually located, so this quadrant identifies the stability region for the two parameters EC and TH. Between 1 s and 0.1 s to locking the TH parameter increases for the six pulses with temperature hollowing (red and green lines), overcoming a threshold indicated by the horizontal line (only marginally for one pulse) and finally in the last 0.1 s to locking also the EC parameter increases for the 6 pulses with edge cooling (green and blues lines), overcoming a threshold indicated by the vertical line. Although it is not the main purpose of this work to develop disruption precursors, this behavior suggest the possibility to find

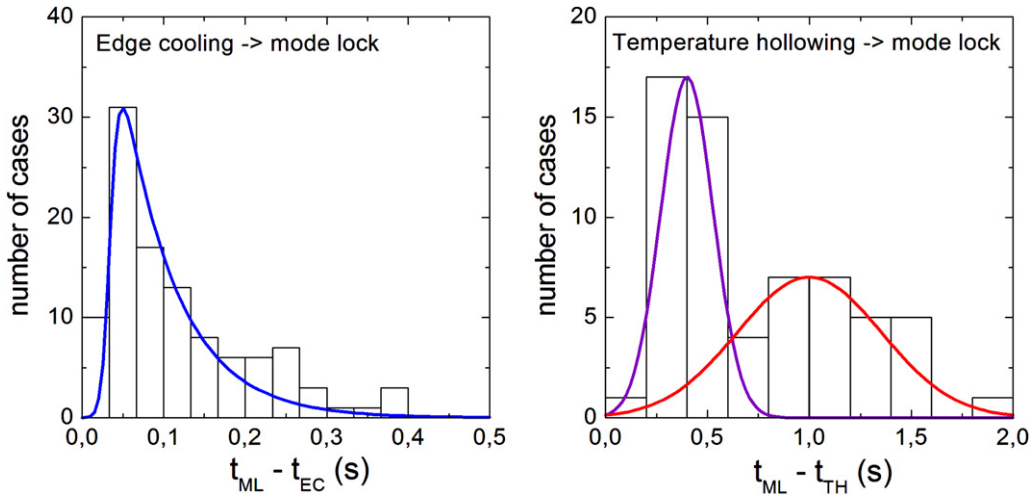

Figure 9. Distribution of the time interval between the increase of parameters EC (t_{EC}, left) and TH (t_{TH}, right) and the locking of the tearing mode (t_{ML}) for the 132 disruptive pulses of the baseline dataset. Solid lines in the plots have been added for sake of visual clarity.

two thresholds for the parameters TH and EC to discriminate between non-disruptive and disruptive pulses and to define alert times based on such parameters. Furthermore, the investigation of possible dependencies of these thresholds on plasma parameters such as plasma current and electron density could help to extrapolate from nowadays devices the thresholds for TH and EC for future reactors, for which disruptions will be unacceptable or reduced as much as possible, thus not allowing the formation of a large database to optimize the threshold values.

4. Characteristic time scales

In order to investigate the characteristic times involved in the evolution of the two parameters TH and EC, the distributions of the time interval between the increase of the parameters and the mode lock have been evaluated for the 132 disruptive pulses of the baseline dataset. Also in this case, the time corresponding to the mode lock has been used as a reference as it is related to the mode growth up to a given amplitude, whilst the time from mode lock to disruption can vary from few milliseconds to hundreds, as shown in figure 8, depending on the mode dynamics and on the logic of the mitigation actions. As it is possible to see in figure 9, the distribution of times to lock for the edge cooling exhibits a characteristic time of the order of 100 ms (left), while the times to lock for the temperature hollowing exhibits a sort of double distribution (right). This behavior can be explained taking into account that the temperature hollowing always precedes the edge cooling in the termination phase of pulses characterized by both processes. The first distribution at lower times (between 200 ms and 600 ms) is probably due to hollowing processes early interrupted by the occurrence of a faster edge cooling. The second distribution (centered around 1 s, also if the reduced number of cases makes the estimation difficult) correspond to pulses with a longer hollowing process, where only the temperature hollowing occurs, or with a later occurrence of edge cooling. The longer delays between the temperature hollowing and the mode lock, compared to delays between the edge cooling and the mode lock, are likely associated, in a first approximation, to the higher resistive diffusion time linking the changes in the electron temperature profile and the changes in the current density profile leading to the mode destabilization.

The characteristic times between the increase of TH and EC and the mode lock shown in figure 9 can be seen as advances of alert times based on the two parameters with respect to mode lock, which is widely adopted as disruption precursor to trigger mitigating actions [46]. In particular, the obtained results indicate that the parameter TH, related to the temperature hollowing, could provide alerts up to 2 s from the mode lock, therefore an attempt to correct the termination avoiding the disruption is possible, e.g. providing central additional heating to counteract the inward transport of high-Z impurities [47, 48]). It is worth noting that, keeping or re-establishing temperature profiles peaked is obviously a clear strategy to avoid these disruptions, but the additional power has to be carefully calibrated to avoid the onset of tearing modes triggered by sawtooth crashes, as observed in pulses characterized by long-period sawtooth activity. The parameter EC, related to the edge cooling, could provide alerts falling within 200 ms from the mode lock, namely not sufficient to correct the termination but enough to anticipate mitigation actions, such as gas injection into the tokamak (leading to a fast loss of thermal energy by photon radiation) [49], to avoid the occurrence of a thermal quench before the DMV intervention.

Additional information with a view to developing disruption precursors based on parameters TH and EC can be provided by the dynamics of $n = 1$ lock mode signals. Assuming that re-establishing temperature profiles peaked providing central additional heating is a clear strategy to avoid disruptions due to temperature hollowing, a differentiated approach could be applied to mitigate disruptions due to edge cooling depending on the shape of the electron temperature profile. As mentioned in section 2.1, mode saturation with peaked electron temperature profile is quite general and usually the thermal quench is induced by DMV intervention (bottom right panel

in figure 3), which is triggered at different time intervals from the mode lock depending on different values of mode lock amplitude and plasma current. For this reason, it is not crucial in this case to anticipate the DMV intervention, which would correspond to inducing a higher current thermal quench. A different behavior is frequently observed when the edge cooling occurs in hollow electron temperature profile, with an explosive growth of the mode amplitude leading in some cases to unmitigated thermal quenches (bottom left panel in figure 6), so it is crucial in this case to anticipate the DMV intervention.

5. Conclusions and perspectives

Tearing modes without evident external triggers are observed in the termination phase of JET pulses in presence of an increased radiation emission in core or edge plasma, leading to temperature hollowing and edge cooling, respectively. These instabilities often lead to a disruption, therefore an analysis of the possible causes of destabilization is of interest toward the optimization of the plasma termination, to reduce the disruption probability or to trigger mitigation actions to reduce the deleterious effects of impending disruptions. A first result shown in this work is that a possible explanation for the mode onset in the termination phase is a linear destabilization as a consequence of changes in the current density profile reflecting the changes in the electron temperature profile. Both temperature hollowing and edge cooling can lead to an unstable MHD scenario, as a consequence of a continuous increase of the current density gradient near the mode resonant surface. This is due to a broadening of the current density profile from inside in the case of temperature hollowing and to a shrinking of the current density profile from outside in the case of edge cooling. After the mode onset, the magnetic island will evolve in the non-linear regime, typically modeled by a MRE.

Following the picture of tearing modes generated by changes in the current density profile, two experimental parameters, TH and EC, have been defined from the electron temperature profile to highlight the occurrence of temperature hollowing and edge cooling and the analysis of a large dataset of pulses carried out in the baseline scenario at JET in the period 2016–2020 led to the introduction of an empirical stability diagram on the plane defined by the two parameters. The possibility to obtain disruption precursors based on the two parameters TH and EC indicating changes in the shape of the electron temperature profile has been preliminary explored, showing that the parameter related to the temperature hollowing could provide alerts useful to attempt to correct the termination avoiding the disruption, whilst the parameter related to the edge cooling could provide alerts useful to anticipate mitigation actions. However, the capability of obtaining alerts well before the mode onset, when stability analysis indicate stable MHD scenarios, are encouraging for future developments. More detailed analysis of the explosive growth of the mode amplitude, frequently observed in pulses with both temperature hollowing and edge cooling and leading in some cases to unmitigated thermal quenches, will be performed in near future also in view of ITER, in whose operations the unmitigated disruption rate should be reduced as much as possible.

Acknowledgments

This work has been carried out within the framework of the EUROfusion Consortium and has received funding from the Euratom research and training programme 2014–2018 and 2019–2020. under Grant agreement No. 633053. The views and opinions expressed herein do not necessarily reflect those of the European Commission.

Appendix A. Analytical modeling

A simple analytical approach is here presented to assess, at first glance, the possible 2/1 mode destabilization as a consequence of changes in the current density profile. As mentioned before, both temperature hollowing and edge cooling can destabilize a $2/1$ tearing mode as a consequence of an increase of the current density gradient near the mode resonant surface. To confirm the destabilization mechanisms, two different sequences of current density profile have been utilized in an analytical form, starting from the same profile, to represent the two cases associated with broadening (in case of temperature hollowing) or shrinking (in case of edge cooling) of the current density profile. The two different paths are intended as the consequence of different radiation increases, involving the core and the edge plasma, respectively. The following parametrization has been used: $j_\phi(\rho) = j_{\phi 0}\left(1-\rho^2\right)^\alpha\left(1+k\rho^2\right)^\beta$, where the parameters $j_{\phi 0}$, α, β and k have been changed taking constant the safety factor at the edge, related to the total plasma current. The results are reported in figure A1 (left) for the cases corresponding to broadening (top) and shrinking (bottom) of the current density profile.

Linear stability analysis have been performed in the zero pressure large aspect ratio approximation by solving the equation for the perturbed radial magnetic field with a shooting-type code for circular flux surfaces equilibria in cylindrical geometry, with a perfectly conducting wall boundary condition. From figure A1 (right) it is possible to see that an increase of the tearing stability index Δ', due to current contributions, is obtained in both cases. For this reason, assuming the neglected stabilizing contributions to be not increasing in the termination phase, being directly proportional to pressure and conductivity (both decreasing), a destabilization mechanism seems to be possible when Δ' exceeds a distinct positive threshold. It is worth noting that the times considered in the two analytical sequences are in arbitrary units, so they may correspond to different time interval in the evolution of current density profile in real pulses and a direct comparison of Δ' values for the two sequences is not possible. The neglected stabilization terms may also be different for pulses characterized by a broadening or a shrinking of the current density profile, respectively, so the obtained results only aim to show the possibility of a destabilization process in the two scenarios.

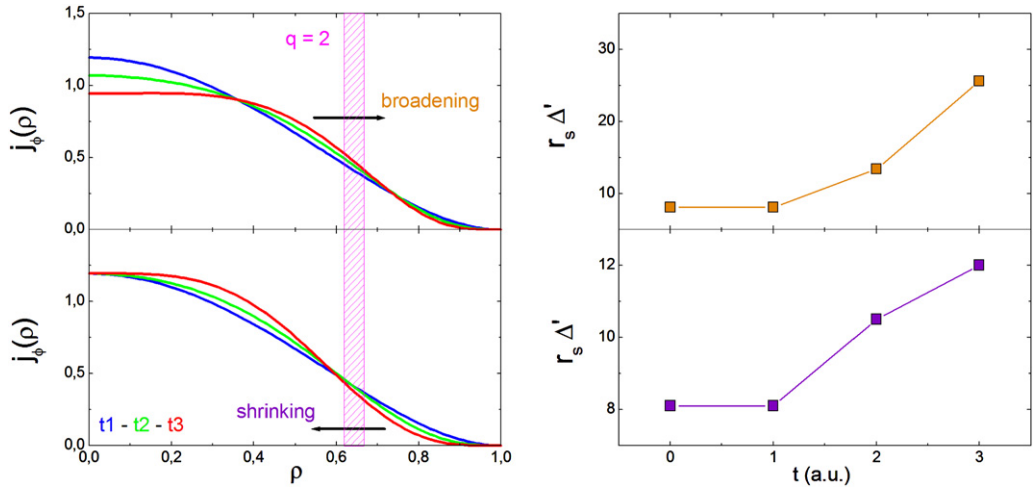

Figure A1. (Left) Time evolution of current density profiles for pulses with broadening (top) and shrinking (bottom) of the current density profile, as obtained by the analytical parametrization reported in the text. (Right) Time evolution of the linear stability parameter Δ' for the two sequences of current density profile reported on the left. The time indicated are in arbitrary units.

ORCID iDs

F. Auriemma https://orcid.org/0000-0002-1043-1563
D. Brunetti https://orcid.org/0000-0001-8650-3271
D.R. Ferreira https://orcid.org/0000-0001-5818-9406
L. Garzotti https://orcid.org/0000-0002-3796-9814
L. Piron https://orcid.org/0000-0002-7928-4661

References

[1] de Vries P.C., Johnson M.F., Alper B., Buratti P., Hender T.C., Koslowski H.R. and Riccardo V. 2011 *Nucl. Fusion* **51** 053018
[2] Cannas B., Fanni A., Murari A., Pau A. and Sias G. 2013 *Plasma Phys. Control. Fusion* **55** 045006
[3] Murari A., Peluso E., Vega J., Gelfusa M., Lungaroni M., Gaudio P. and Martínez F.J. 2017 *Nucl. Fusion* **57** 016024
[4] Pau A., Fanni A., Carcangiu S., Cannas B., Sias G., Murari A. and Rimini F. 2019 *Nucl. Fusion* **59** 106017
[5] Kates-Harbeck J., Svyatkovskiy A. and Tang W. 2019 *Nature* **568** 526
[6] Furth H.P., Killeen J. and Rosenbluth M.N. 1963 *Phys. Fluids* **6** 459
[7] de Vries P.C. *et al* 2014 *Phys. Plasmas* **21** 056101
[8] Sykes A. and Wesson J.A. 1980 *Phys. Rev. Lett.* **44** 1215
[9] Wesson J.A. *et al* 1989 *Nucl. Fusion* **29** 641
[10] Hobirk J. *et al* 2018 *Nucl. Fusion* **58** 076027
[11] Pucella G., Botrugno A., Buratti P., Giovannozzi E., Marinucci M. and Tudisco O. 2013 *Proc. 40th EPS Conf. on Plasma Physics* (1-5 July 2013 Espoo, Finland) vol 37D (ECA) P5.139 (http://ocs.ciemat.es/EPS2013PAP/pdf/P5.139.pdf)
[12] Nave M.F.F. and Wesson J.A. 1990 *Nucl. Fusion* **30** 2575
[13] Adler E.A., Kulsrud R.M. and White R.B. 1980 *Phys. Fluids* **23** 1375
[14] Shafranov V.D. *et al* 1970 *Sov. Phys.-Tech. Phys.* **15** 175
[15] Strauss H.R. 1981 *Phys. Fluids* **24** 2004
[16] Hegna C.C. and Callen J.D. 1994 *Phys. Plasmas* **1** 2308
[17] Joffrin E. *et al* 2014 *Nucl. Fusion* **54** 013011
[18] Wesson J.A. 2004 *Tokamaks* 3rd edn (Oxford: Oxford University Press)
[19] Nardone C. 1992 *Plasma Phys. Control. Fusion* **34** 1447
[20] Hawryluk R J 1980 *Physics of Plasmas Close to Thermonuclear Conditions* ed B. Coppi vol 1 (Brussels: CEC) p 19
[21] Lao L.L., St. John H., Stambaugh R.D., Kellman A.G. and Pfeiffer W. 1985 *Nucl. Fusion* **25** 1611
[22] LoDestro L.L. and Pearlstein L.D. 1994 *Phys. Plasmas* **1** 90
[23] Keeling D.L., Challis C.D., Jenkins I., Hawkes N.C., Lupelli I., Michael C. and de Bock M.F.M. 2018 *Nucl. Fusion* **58** 016028
[24] Kim H.-T. *et al* 2020 *Nucl. Fusion* **60** 066003
[25] Brunetti D., Lazzaro E., Nowak S., Sauter O. and Graves J.P. 2016 *J. Phys.: Conf. Ser.* **775** 012002
[26] Lütjens H., Bondeson A. and Sauter O. 1996 *Comput. Phys. Commun.* **97** 219
[27] Furth H.P., Rutherford P.H. and Selberg H. 1973 *Phys. Fluids* **16** 1054
[28] Glasser A.H., Greene J.M. and Johnson J.L. 1975 *Phys. Fluids* **18** 875
[29] Glasser A.H., Greene J.M. and Johnson J.L. 1976 *Phys. Fluids* **19** 567
[30] Nishimura Y., Callen J.D. and Hegna C.C. 1998 *Phys. Plasmas* **5** 4292
[31] White R.B. 1986 *Rev. Mod. Phys.* **58** 183
[32] Drake J.F., Antonsen T.M. Jr, Hassam A.B. and Gladd N.T. 1983 *Phys. Fluids* **26** 2509
[33] Rutherford P.H. 1973 *Phys. Fluids* **16** 1903
[34] White R.B., Monticello D.A., Rosenbluth M.N. and Waddell B.V. 1977 *Phys. Fluids* **20** 800
[35] Rutherford P.H. 1985 Princeton Plasma Physics Labotory Report (Princeton, NJ: Princeton University) vol 2277 (inis.iaea.org/collection/NCLCollectionStore/_Public/17/026/17026389.pdf)
[36] Bishop C.M., Connor J.W., Hastie R.J. and Cowley S.C. 1991 *Plasma Phys. Control. Fusion* **33** 389
[37] Gorelenkov N.N., Budny R.V., Chang Z., Gorelenkova M.V. and Zakharov L.E. 1996 *Phys. Plasmas* **3** 3379
[38] Rebut P.H. and Hugon M. 1985 *Proc. 10th Int. Conf. on Plasma Physics and Controlled Nuclear Fusion Research 1984* (12-19 September 1984 London, United Kingdom) (IAEA, Vienna, 1985) vol 2 IAEA-CN-44/E-III-7 (www-naweb.iaea.org/napc/physics/FEC/STIPUB670_VOL2.pdf) p 197
[39] Salzedas F., Schüller F.C. and Oomens A.A.M. 2002 *Phys. Rev. Lett.* **88** 075002
[40] Gates D.A. and Delgado-Aparicio L. 2012 *Phys. Rev. Lett.* **108** 165004

[41] Gates D.A., Delgado-Aparicio L. and White R.B. 2013 *Nucl. Fusion* **53** 063008
[42] White R.B., Gates D.A. and Brennan D.P. 2015 *Phys. Plasmas* **22** 022514
[43] Teng Q., Brennan D.P., Delgado-Aparicio L., Gates D.A., Swerdlow J. and White R.B. 2016 *Nucl. Fusion* **56** 106001
[44] Xu L. *et al* 2017 *Nucl. Fusion* **57** 126002
[45] Garzotti L. *et al* 2019 *Nucl. Fusion* **59** 076037
[46] de Vries P.C. *et al* 2016 *Nucl. Fusion* **56** 026007
[47] Dux R., Neu R., Peeters A.G., Pereverzev G., Mück A., Ryter F. and Stober J. (ASDEX Upgrade Team) 2003 *Plasma Phys. Control. Fusion* **45** 1815
[48] Valisa M. *et al* 2011 *Nucl. Fusion* **51** 033002
[49] Lehnen M. *et al* 2011 *Nucl. Fusion* **51** 123010